Supporting Information

Unraveling a Biomass-Derived Multiphase Catalyst for the Dehydrogenative Coupling of Silanes with Alcohols under Aerobic Conditions

Iván Sorribes,[a,†] David Ventura-Espinosa,[b] Marcelo Assis,[c] Santiago Martín,[d,e] Patricia Concepción,[f] Jefferson Bettini,[g] Elson Longo,[c] Jose A. Mata,[b] Juan Andrés[a]*

[a]Departament de Química Física i Analítica, Universitat Jaume I, 12071 Castellón, Spain
[b]Institute of Advanced Materials (INAM), Universitat Jaume I, 12071, Castellón, Spain
[c]Center for Development of Functional Materials (CDMF), Federal University of São Carlos, 13565-905 São Carlos, SP, Brazil
[d]Instituto de Nanociencia y Materiales de Aragón (INMA), CSIC-Universidad de Zaragoza, 50009 Zaragoza, Spain
[e]Departamento de Química Fisica, Universidad de Zaragoza, 50009 Zaragoza, Spain
[f]Instituto de Tecnología Química, Universitat Politècnica de València-Consejo Superior de Investigaciones Científicas, 46022 Valencia, Spain
[g]Brazilian Nanotechnology National Laboratory (LNNano), 13083-970 Campinas, Brazil
[†]Present address: Instituto de Tecnología Química, Universitat Politècnica de València-Consejo Superior de Investigaciones Científicas, 46022 Valencia, Spain

* Corresponding author. Email addresses: isorribe@uji.es, ivsorter@itq.upv.es

Number of pages: 25
Number of figures: 17
Number of tables: 1

1. METAL COMPOSITION OF Ag AND/OR Cr CONTAINING CATALYSTS

Table S1. Metal composition of prepared catalysts determined by ICP-MS analysis.

Catalyst	Ag (wt %)	Cr (wt %)	Ag + Cr (wt %)	Ag/Cr ratio
AgCr@CN-400	10.84	2.88	13.72	3.76
AgCr@CN-500	11.41	3.08	14.49	3.70
AgCr@CN-600	11.59	3.12	14.71	3.71
AgCr@CN-700	11.95	3.20	15.15	3.73
AgCr@CN-800	12.74	3.40	16.14	3.74
AgCr@CN-900	14.16	3.82	17.98	3.70
M-free@CN-800	-	-	-	-
AgCr@CN-800-acid	0.12	2.29	2.41	0.05
Ag@CN-800	14.41	-	14.41	-
Ag@CN-800-acid	0.13	-	0.13	-
Cr@CN-800-acid	-	2.40	2.40	-

2. EXTENSION DATA OF CATALYTIC STUDIES FOR CATALYSTS AgCr@CN-X (X = 400-900 ºC), M-free@CN-800, AgV@CN-800, AND AgW@CN-800

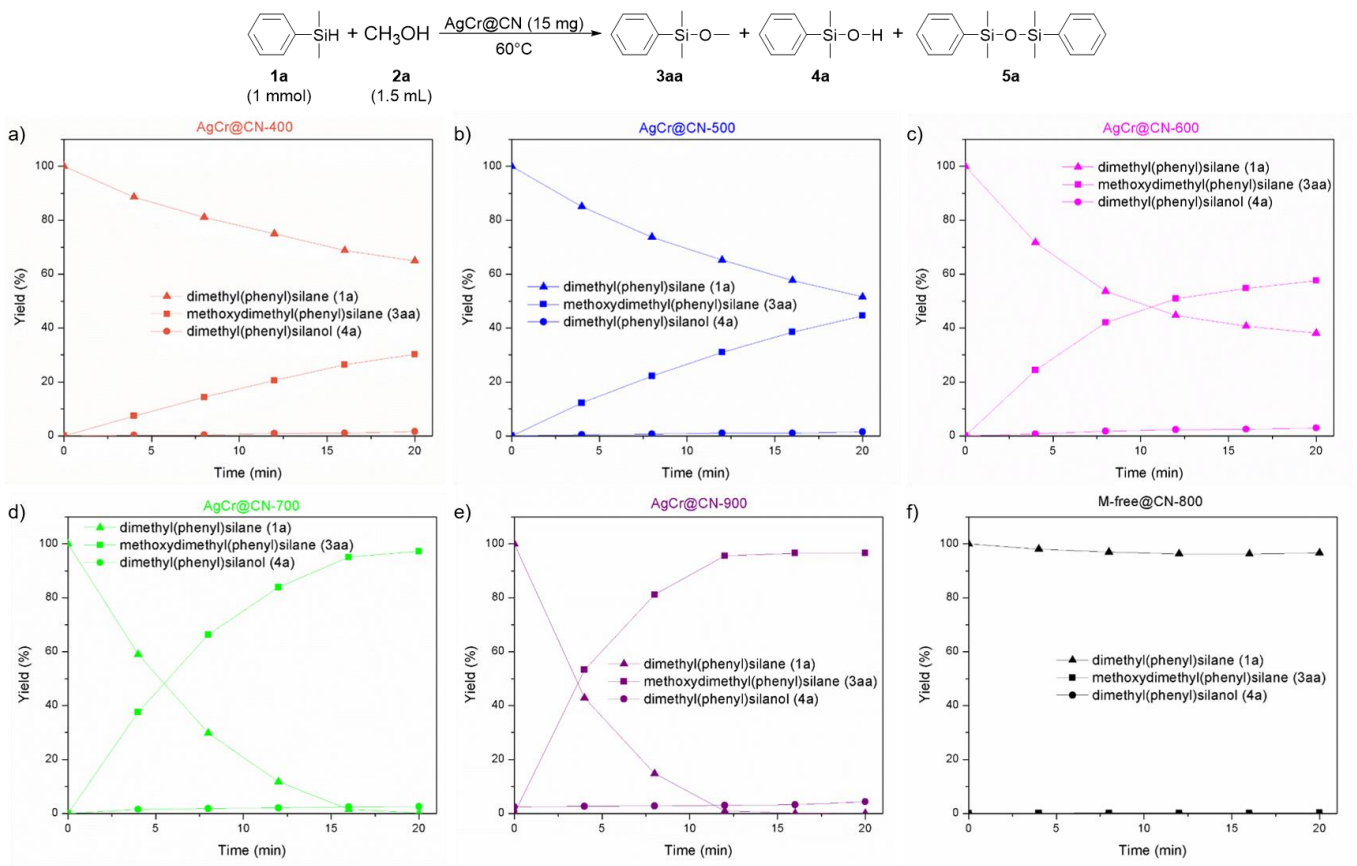

Figure S1. Concentration/time diagram for the dehydrogenative coupling reaction of **1a** with methanol in the presence of (a) AgCr@CN-400, (b) AgCr@CN-500, (c) AgCr@CN-600, (d) AgCr@CN-700, (e) AgCr@CN-900, and (f) M-free@CN-800.

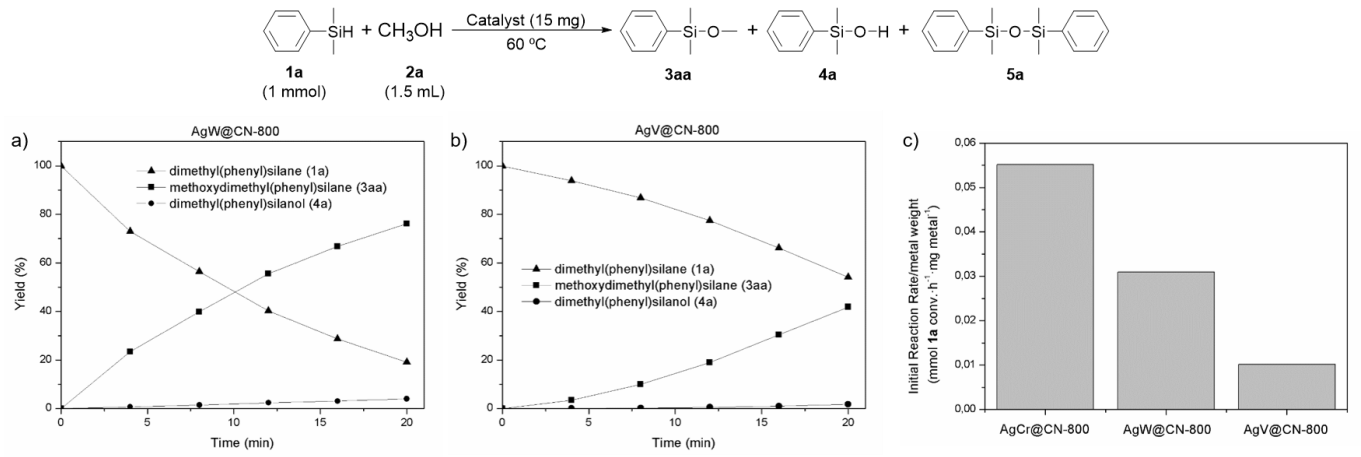

Figure S2. Concentration/time diagram for the dehydrogenative coupling reaction of **1a** with methanol in the presence of (a) AgW@CN-800 (14.26 metal wt %), (b) AgV@CN-800 (9.76 metal wt %). (c) Comparison of the metal mass activity of different silver containing bimetallic catalyst prepared by the chitosan-annealing synthetic approach.

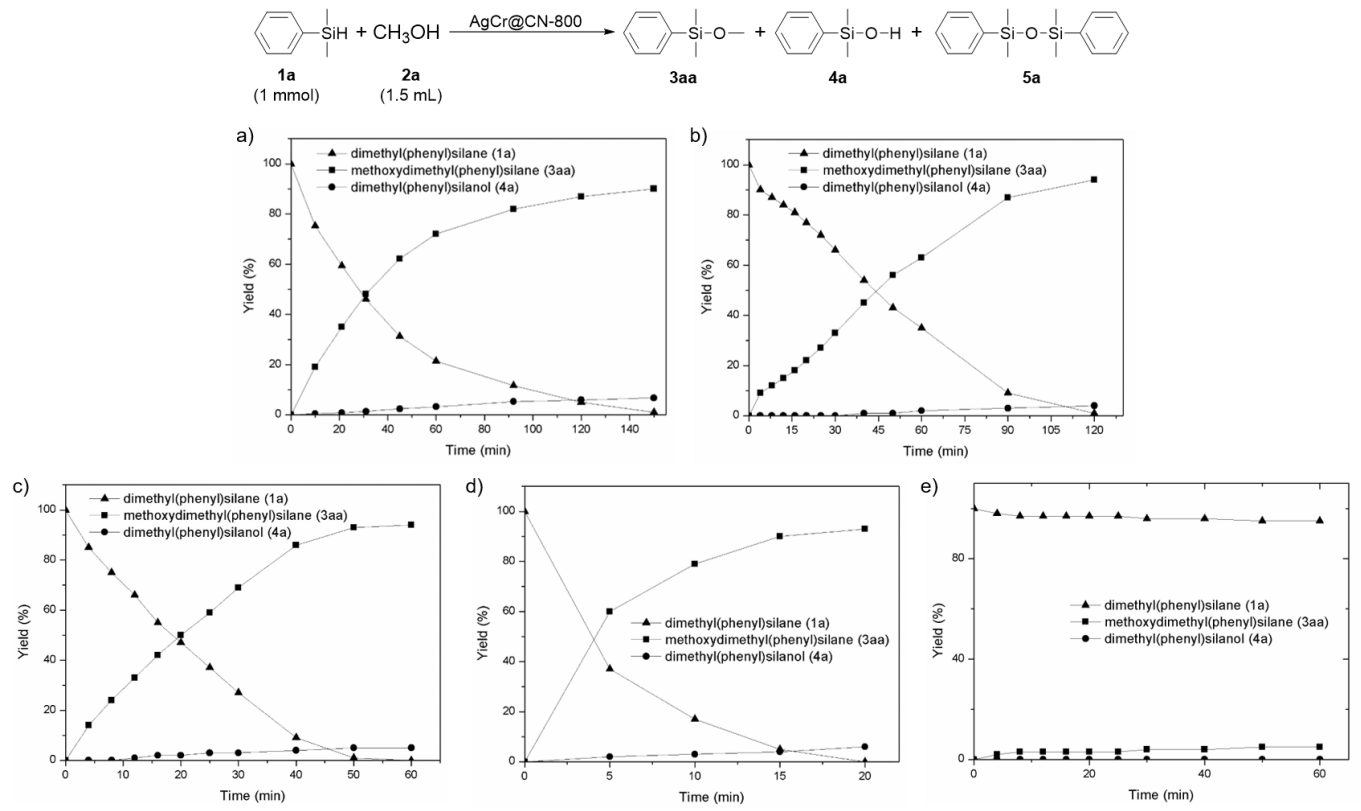

Figure S3. Concentration/time diagram for the dehydrogenative coupling reaction of **1a** with methanol in the presence of catalyst AgCr@CN-800. Reaction conditions: (a) AgCr@CN-800 (5 mg), 60 ºC; (b) AgCr@CN-800 (15 mg), 0 ºC. (c) AgCr@CN-800 (15 mg), 30 ºC. (d) AgCr@CN-800 (15 mg), 30 ºC, O_2 bubbling. (e) AgCr@CN-800 (15 mg), 30 ºC, Ar atmosphere.

Turnover number (TON) and Turnover Frequency (TOF)

$$TON = \frac{mol\ conv.\ \mathbf{1a}}{mol\ Ag + mol\ Cr} = \frac{1}{0{,}009} = 111 \qquad \text{(Eq. S1)}$$

$$TOF = \frac{(mol\ conv.\ \mathbf{1a}/mol\ Ag + mol\ Cr)}{time} = \frac{1 \cdot 0{,}15 / 0{,}0275}{1/60} = 327\ h^{-1} \qquad \text{(Eq. S2)}$$

Procedure for the measurement of the H_2 evolution for the dehydrogenative coupling reaction of dimethyl(phenyl)silane (1a) and methanol

A 4 mL vial containing 15 mg of AgCr@CN-800, anisole as an internal standard (0.5 mmol), anhydrous methanol (1.0 mL), and a stirring bar was introduced in a 500 mL flat-bottom flask. Once the flat-bottom flask was sealed with a septum, the silane **1a** (1 mmol) was added through a syringe together with an additional amount of anhydrous methanol (0.5 mL), basically used to collect the remaining amount of silane inside the syringe. Then, the reaction mixture was stirred at 25 ºC (laboratory temperature) and when the reaction was finished, the evolved H_2 gas was released in a measure setup consisting in an inverted burette system. A blank in the absence of catalyst was also carried to avoid measurement errors. The volume of H_2 gas evolved ($V_{H2} - V_{blank}$) was 24.3 mL, which according to the Van der Waals equation shown below is equivalent to 1 mmol of H_2.

$$V_m = \frac{RT}{p} + b - \frac{a}{RT} = 24{,}45\ \frac{L}{mol} \qquad \text{(Eq. S3)}$$

$R = 8{,}3145\ m^3 \cdot Pa \cdot mol^{-1}$
$T = 298\ K$
$p = 101{,}325\ Pa$
$a = 2{,}49 \cdot 10^{-10}\ Pa \cdot m^3 \cdot mol^{-2}$
$b = 26{,}7 \cdot 10^{-6}\ m^3 \cdot mol^{-1}$

3. EXTENSION OF THE CHARACTERIZATION RESULTS FOR CATALYST AgCr@CN-800

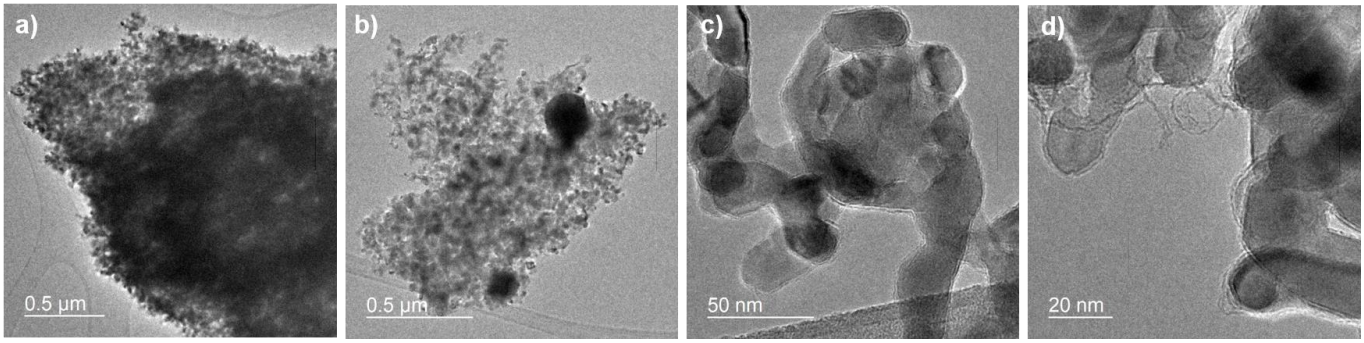

Figure S4. TEM images of catalyst AgCr@CN-800.

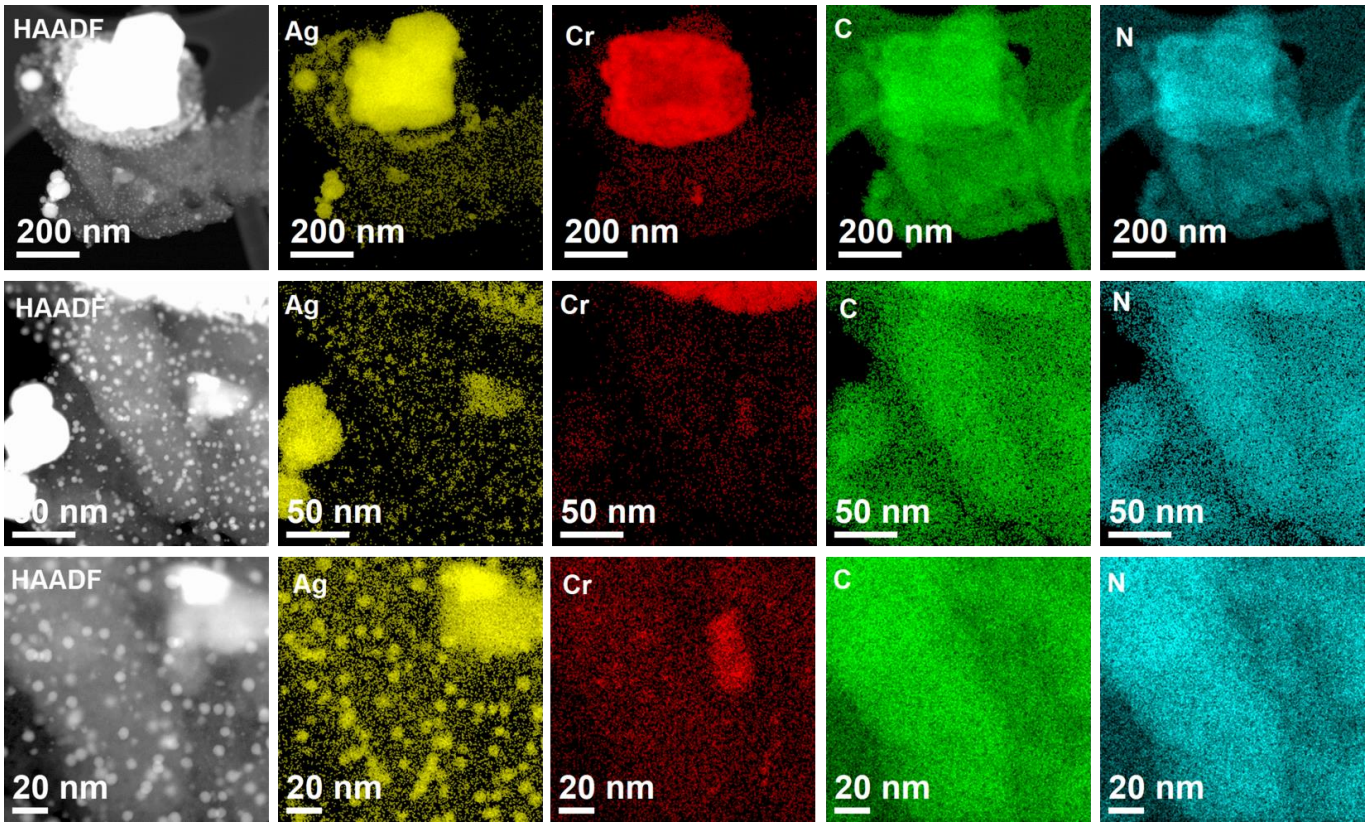

Figure S5. EDS elemental mapping of Ag, Cr, C, and N for catalyst AgCr@CN-800.

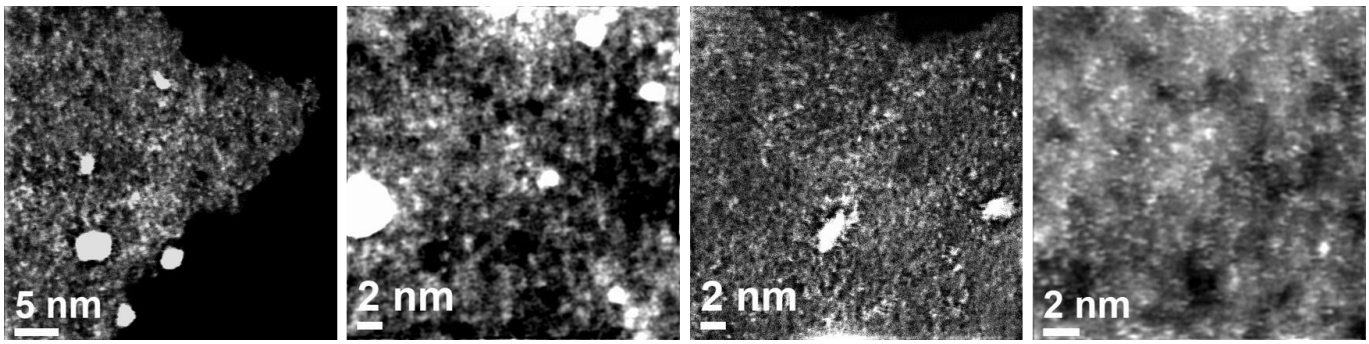

Figure S6. High-magnification images of the Cs-corrected HAADF-STEM analysis for catalyst AgCr@CN-800.

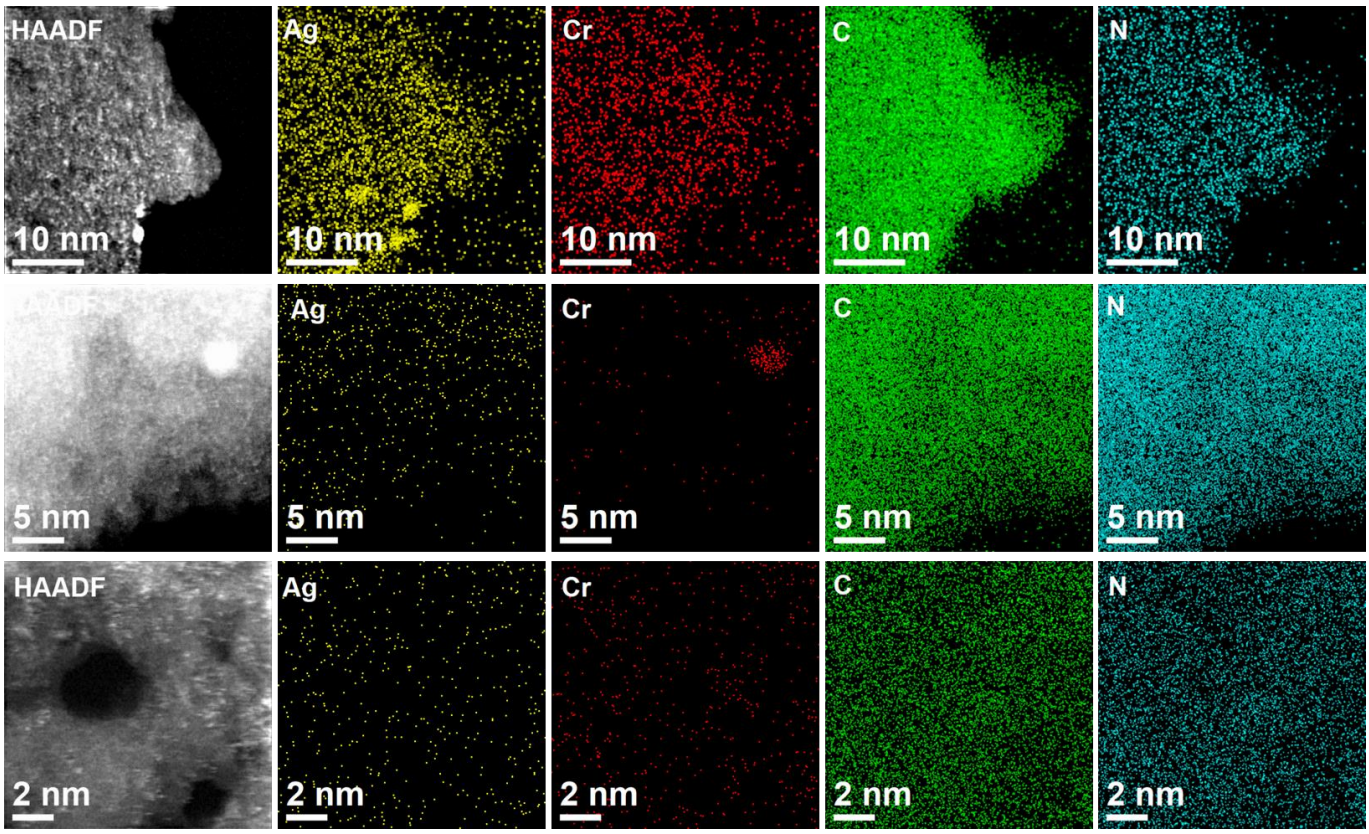

Figure S7. High-magnification EDS elemental mapping of Ag, Cr, C, and N for catalyst AgCr@CN-800.

4. CHARACTERIZATION RESULTS AND CATALYTIC STUDIES FOR CATALYST AgCr@CN-800-Ar

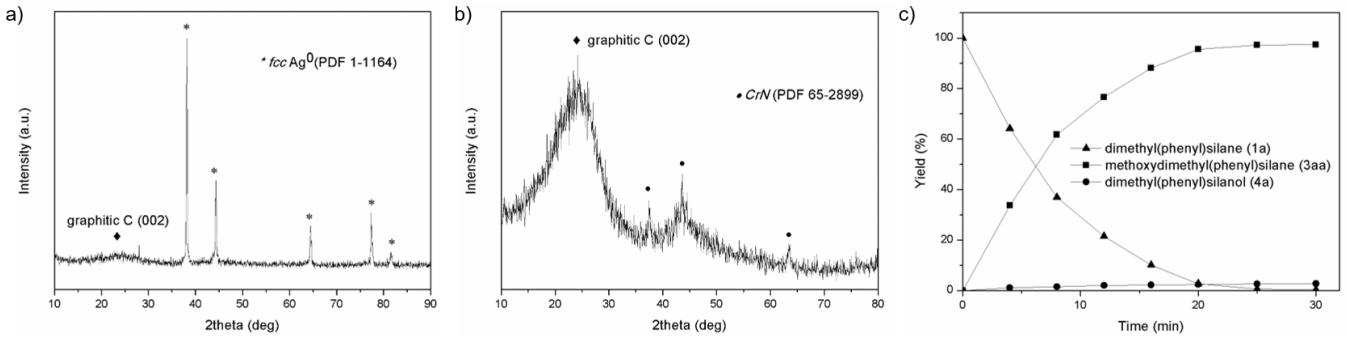

Figure S8. XRD pattern of catalyst AgCr@CN-800-Ar (a) and AgCr@CN-800-Ar-Acid (b). (c) Concentration/time diagram for the dehydrogenative coupling reaction of **1a** with methanol in the presence of catalyst AgCr@CN-800-Ar.

5. CHARACTERIZATION RESULTS AND CATALYTIC STUDIES FOR CATALYST Ag@CN-800

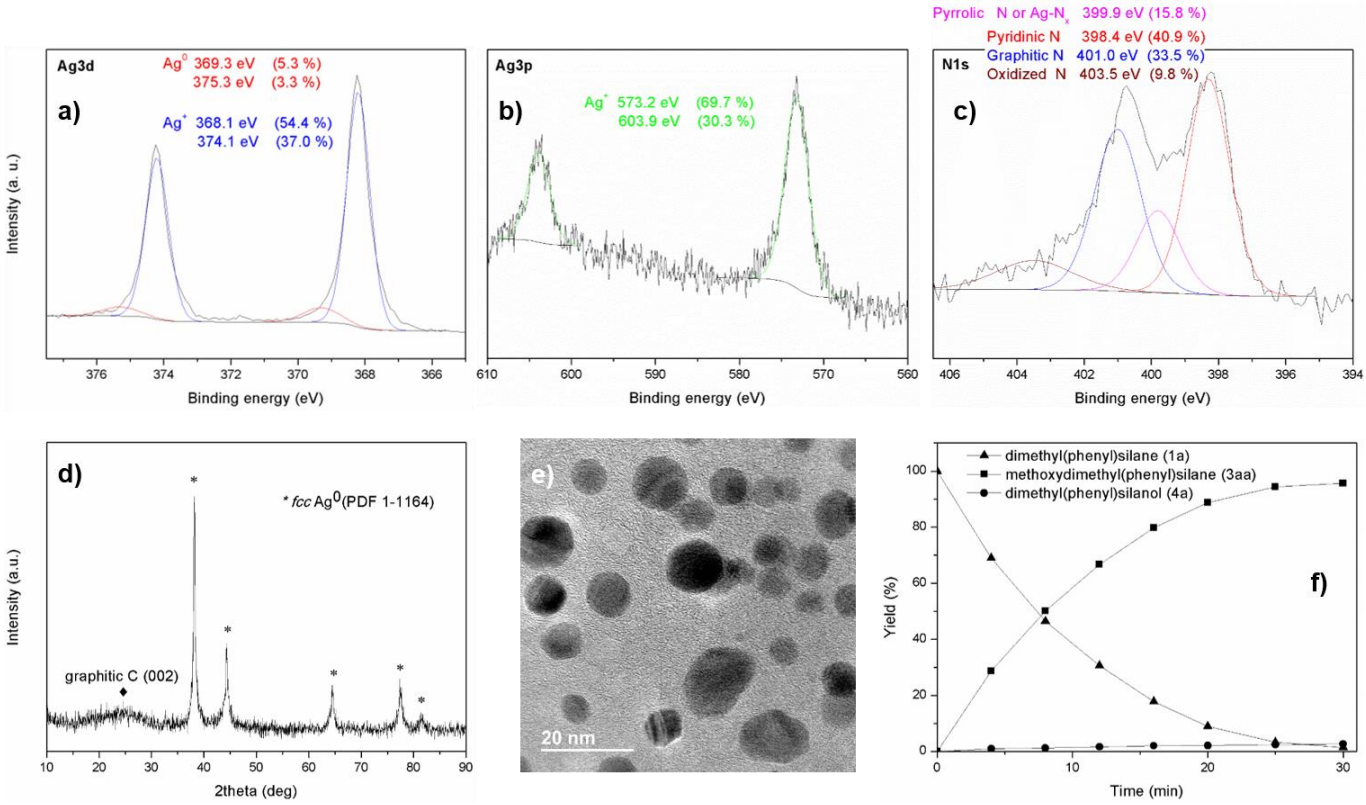

Figure S9. Characterization of catalyst Ag@CN-800. Ag 3d (a), Ag 3p (b) and N 1s (c) core level XPS spectra. (d) XRD pattern. (e) TEM image. (f) Concentration/time diagram for the dehydrogenative coupling reaction of **1a** with methanol in the presence of catalyst Ag@CN-800.

The XRD pattern (Figure S9d) of catalyst Ag@CN-800 presents the diffraction peaks associated with the face-centered cubic (*fcc*) structure of Ag^0 in agreement with the JCPDS database (PDF Card 1-1164). The high-resolution Ag 3d core level XPS spectrum (Figure S9a) displays two peaks associated with the characteristic spin–orbit splitting of Ag $3d_{5/2}$ and Ag $3d_{3/2}$ orbitals. Each of these peaks can be fitted into two separated components, the ones associated with Ag^+ species (at 368.1 and 374.1 eV) and the components associated with Ag^0 (at 369.3 and 375.3 eV). As shown in Figure S9b, the characteristic peaks associated with Ag^0 species are also present in the high-resolution Ag 3p core level spectrum. Importantly, as it is mentioned in the main manuscript for catalyst AgCr@CN-800, the obtained binding energy values for Ag^+ species compared with those of molecular-defined complexes, which contain Ag-N bonds within a related structure (368.4 eV),[1] revealed a prominent increase of their electron density according to previous comparison studies reported in the literature.[2] This result suggests that these Ag^+ species could be embedded in N-doped graphitic carbon in the form of Ag-N_x sites. This suggestion is also supported by the results obtained from the comparison of the high-resolution N 1s energy level spectrum (Figure S9c) with that of the catalyst M-free@CN-800 (Figure 4d). More specifically, there is

an energy shift of over 0.2 eV in the pyridinic-N component as result of the existence of Ag-N interactions.[2-4] Moreover, there is an increase of the ratio of pyrrolic-N to pyridinic-N species, which could be associated with the presence of Ag^+ species attached to pyridinic-N that results in the formation of Ag-N_x species, whose binding energies fall in the same range as the pyrrolic-N function binding energy. On the whole, catalyst Ag@CN-800 is constituted by crystalline nanoparticles with a narrow size distribution of 5-20 nm (as shown in Figure S9e) embedded in N-doped graphitic structures that contain highly dispersed Ag-N_x sites as well.

6. CHARACTERIZATION OF CATALYST Ag@CN-800-Acid

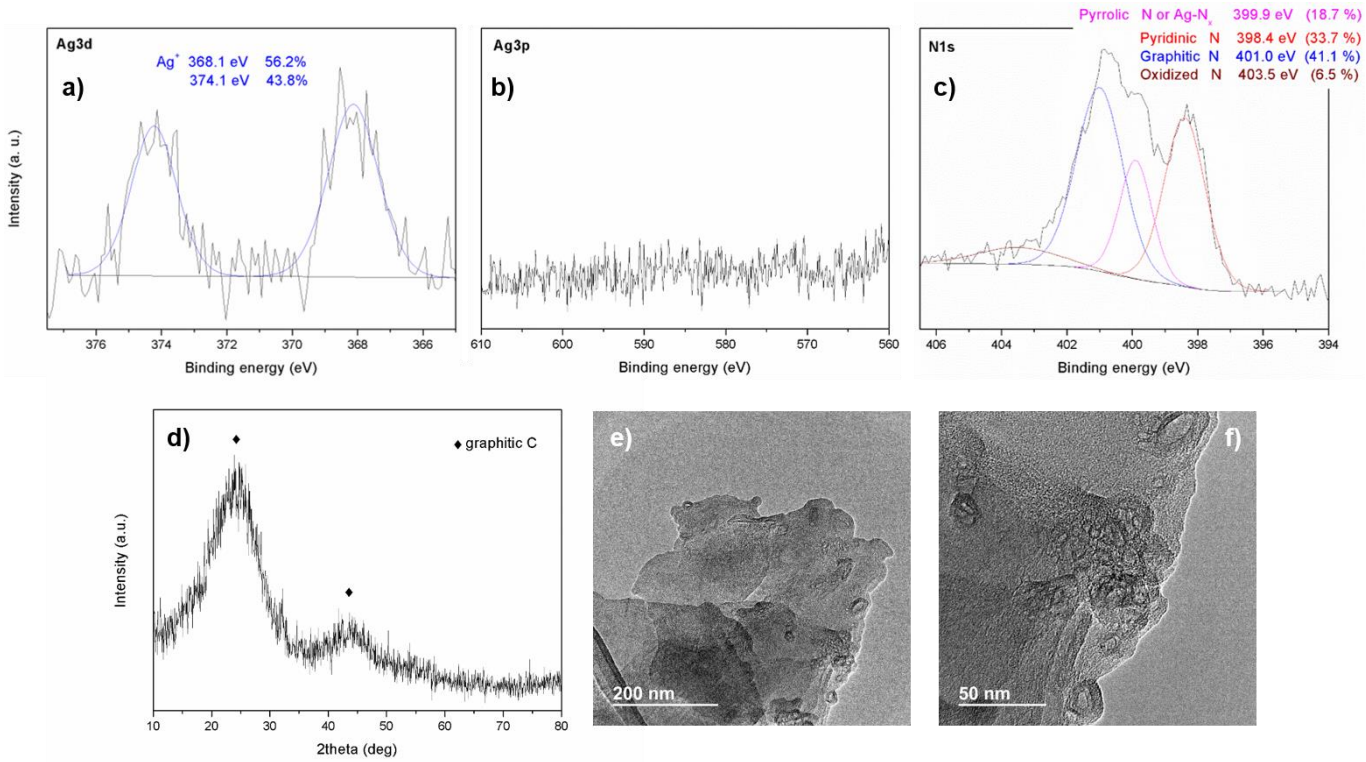

Figure S10. Characterization of catalyst Ag@CN-800-Acid. Ag 3d (a), Ag 3p (b) and N 1s (c) core level XPS spectra. (d) XRD pattern. (e, f) TEM images.

The high-resolution Ag 3d core level spectrum (Figure S10a) of catalyst Ag@CN-800-Acid displays the two characteristic peaks associated with the spin–orbit splitting of Ag $3d_{5/2}$ and Ag $3d_{3/2}$ orbitals. However, compared with the XPS spectrum of catalyst Ag@CN-800, each of these peaks can only be fitted into one component associated with Ag^+ species at exactly the same binding energies of 368.1 and 374.1 eV. Moreover, a silent high-resolution Ag 3p core level XPS spectrum is obtained (Figure S10b), further confirming the absence of Ag^0 species. The N 1s XPS spectrum (Figure S10c) is similar to the one of catalyst Ag@CN-800. No other diffraction peaks different to the ones associated with graphitic carbon are observed in the XRD pattern (Figure S10d) of the acid-etched catalyst Ag@CN-800-Acid. As shown in Figures S10e-f, TEM images (Figures S10e-f) show no particles while the hollow-centered graphitic

carbon layers are still preserved. All these characterization results (see also Table S1) confirm that the consecutive acid leaching treatments effectively remove the Ag metallic nanoparticles from catalyst Ag@CN-800, and consequently, the acid-etched catalyst Ag@CN-800-Acid is only constituted by highly dispersed Ag-N_x sites embedded in N-doped graphitic carbon.

7. CHARACTERIZATION OF CATALYST Cr@CN-800-Acid

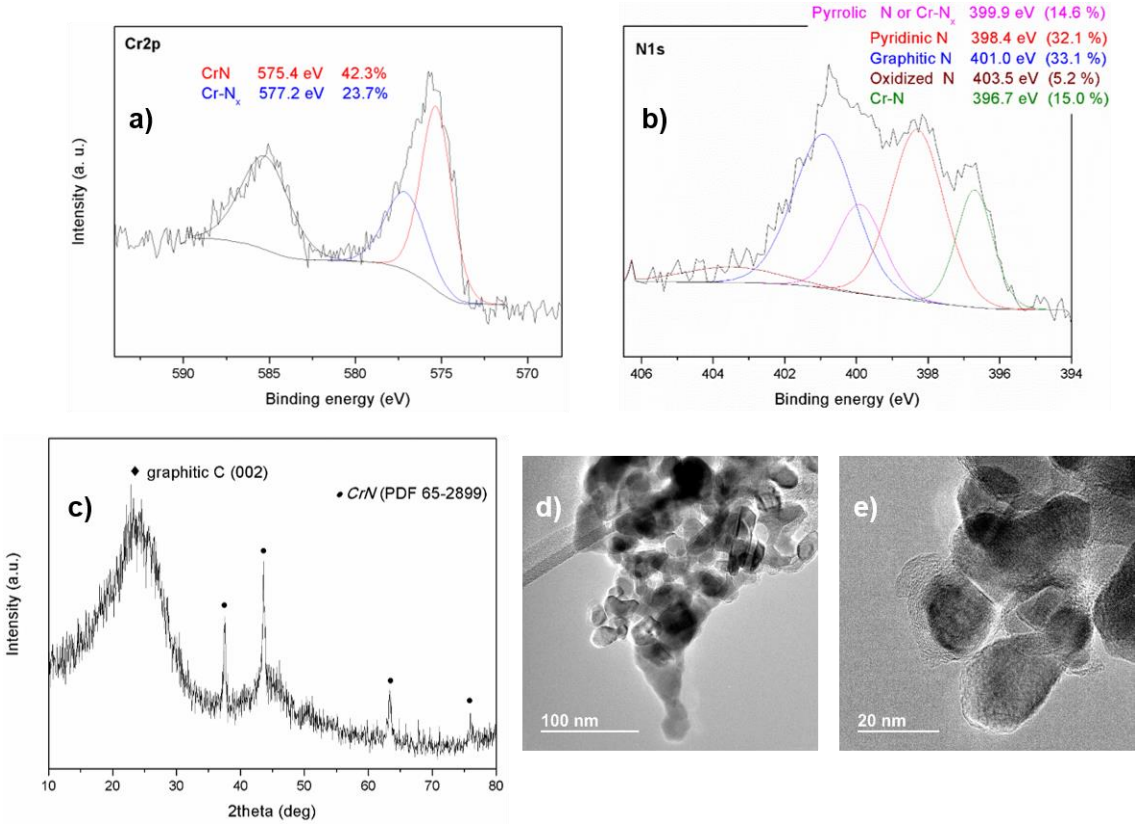

Figure S11. Characterization of catalyst Cr@CN-800-Acid. Cr 2p (a), and N 1s (b) core level XPS spectra. (c) XRD pattern. (d, e) TEM images.

The XRD pattern of catalyst Cr@CN-800-Acid (Figure S11c) shows diffraction peaks associated with the cubic phase of CrN (PDF Card 65-2899) as well as the characteristic broad ones of graphitic carbon. As reveled by TEM characterization (Figure S11d-e), CrN is in the form of crystalline nanoparticles (~ 30 nm) coated by (defect/N-doped) graphitic carbon layers. Besides the four types of N species, characteristic of N-doped graphitic materials (i.e. pyridinic N-oxide, graphitic-N, pyrrolic-N, and pyridinic-N), the component (at 396.7 eV) attributed to CrN can also be inferred in the high-resolution N 1s core level XPS spectrum (Figure S11b). Importantly, an energy shift of over 0.2 eV of the pyridinic-N component with respect to the one of catalyst M-free@CN-800 (Figure 4d) can also be detected,[2-4] thus suggesting the existence of Cr-N_x sites, whose binding energies fall in the same range as the pyrrolic-N function binding energy. Furthermore, the components of both CrN and atomically dispersed Cr-N_x sites can also be observed in the high-resolution Cr 2p XPS spectrum of catalyst Cr@CN-Acid after deconvolution and fitting (Figure S11a).

8. KINTETIC STUDIES

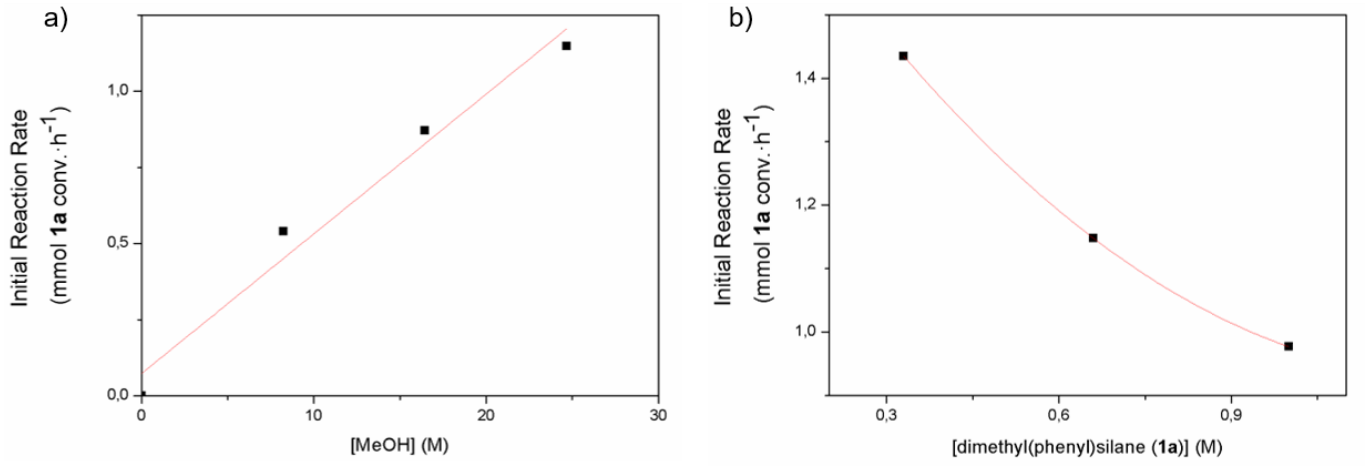

Figure S12. Kinetic studies on the dehydrogenative coupling reaction of **1a** with methanol in the presence of catalyst AgCr@CN-800. (a) Initial reaction rate at different concentrations of methanol. Reaction conditions: 10 mg AgCr@CN-800, **1a** (1 mmol), solvent (methanol + ethyl acetate = 1.5 mL), 0.5 mmol anisole as an internal standard, 30 ºC.

(b) Initial reaction rate at different concentrations of dimethyl(phenyl)silane (**1a**). Reaction conditions: 10 mg AgCr@CN-800, methanol (1.5 mL), 0.5 mmol anisole as an internal standard, 30 ºC.

9. EXTENSION OF RAMAN SPECTROSCOPY INVESTIGATIONS

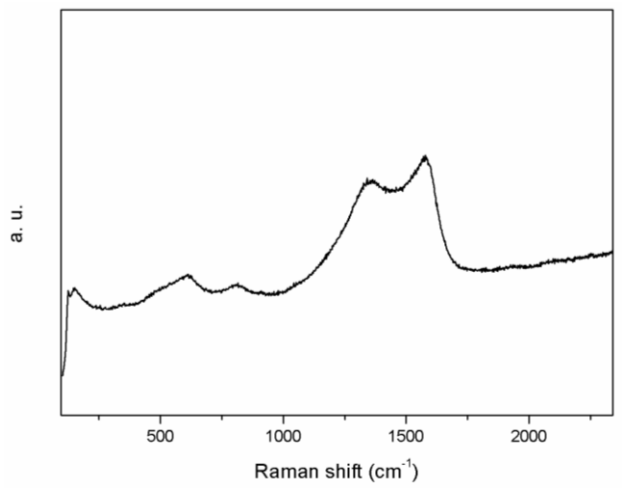

Figure S13. (a) Raman spectrum on catalyst AgCr@CN-800 in an Ar flow at room temperature.

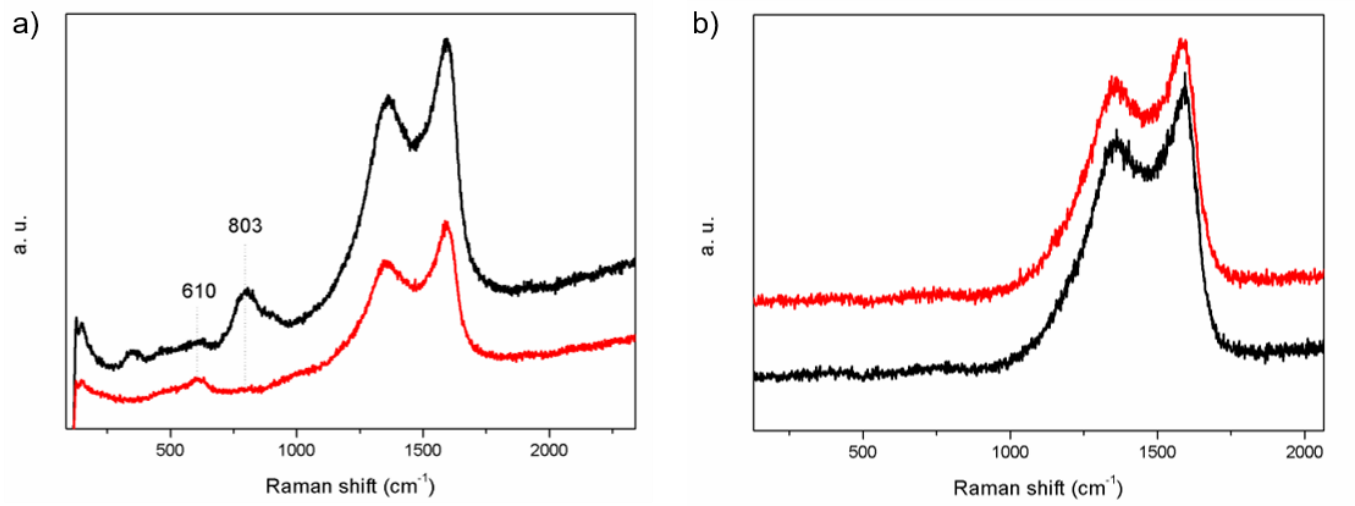

Figure S14. (a) Evolution of the bands in the Raman spectra on catalyst AgCr@CN-800 after sequentially dosing at room temperature a 20% O_2/Ar flow (black line) and a silane **1a**/Ar flow (red line). (b) Raman spectra of catalyst AgCr@CN-800 after sequentially dosing at room temperature a H_2 flow (black line) and a methanol/Ar flow (red line).

10. HOT FILTRATION EXPERIMENT

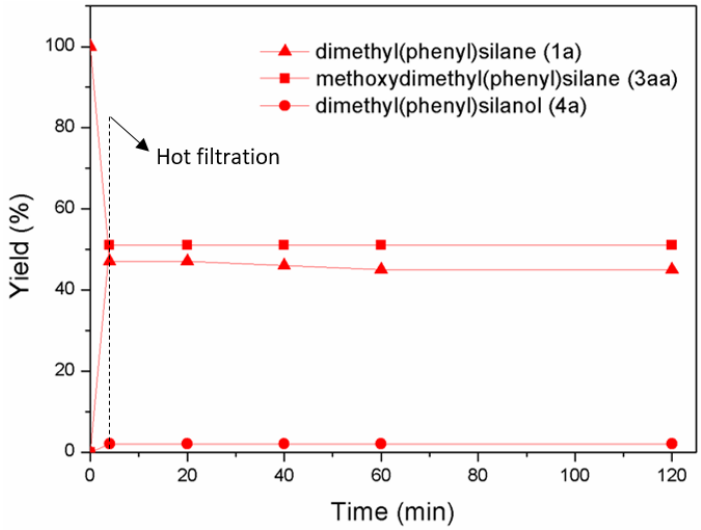

Figure S15. Hot filtration experiment. Reaction conditions: **1a** (1 mmol), methanol (1.5 mL), catalyst AgCr@CN-800 (15 mg), 60 ºC, and after filtration 30 ºC. Yields determined by GC using anisole as an internal standard (54 µL, 0.5 mmol).

11. CHARACTERIZATION OF THE RECYCLED CATALYST AgCr@CN-800-R4

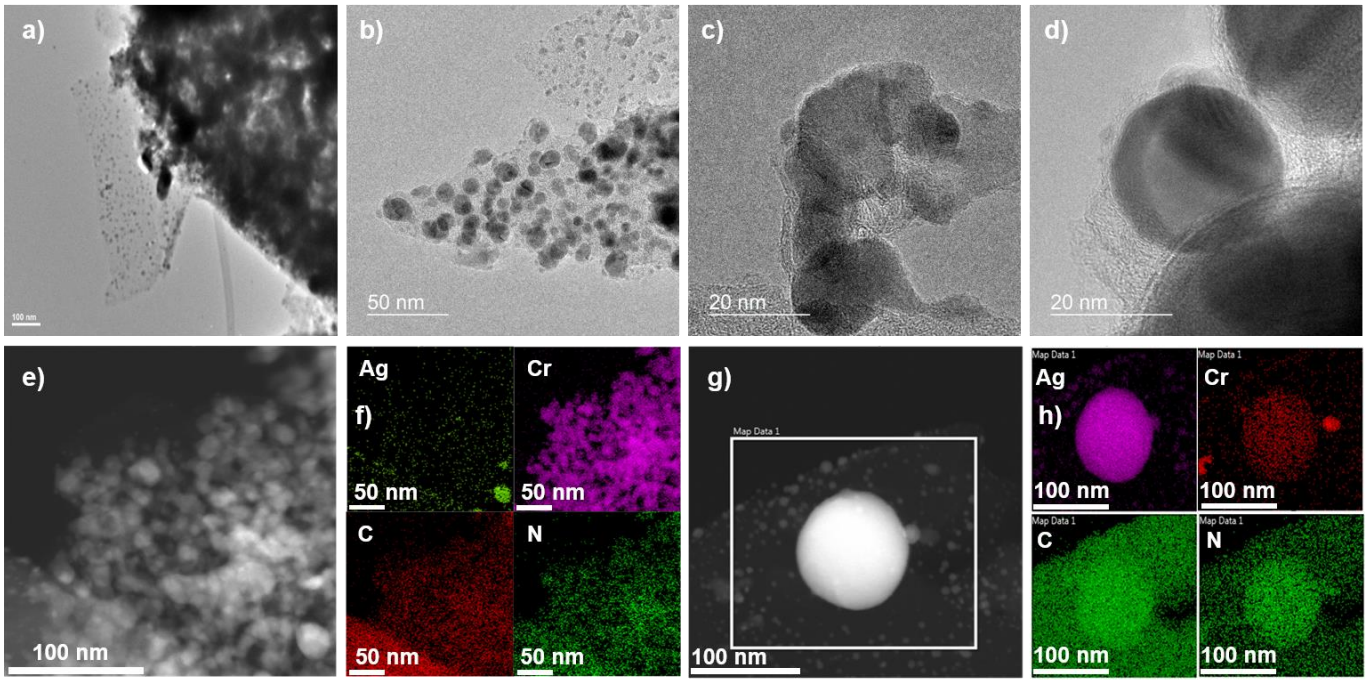

Figure S16. TEM (a, b), HRTEM (c, d) and HAADF-STEM (e, g) images of the recycled catalyst AgCr@CN-800-R4. (f, h) EDS elemental mapping for Ag, Cr, C, and N.

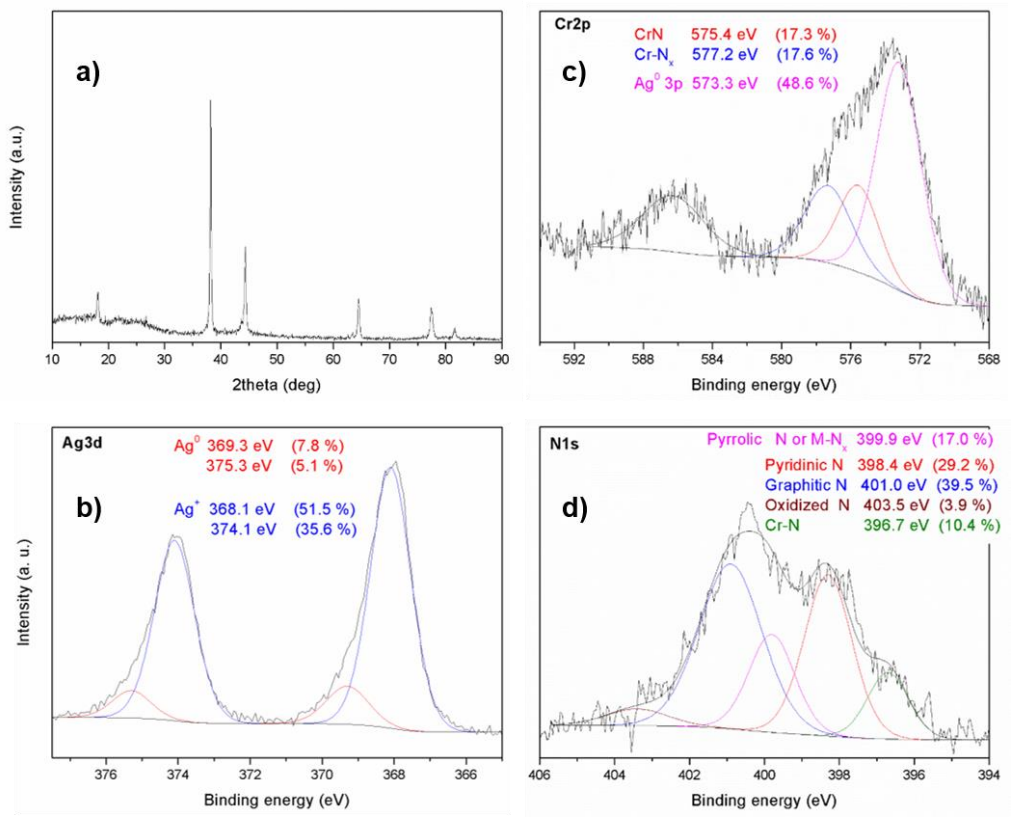

Figure S17. XRD pattern (a), and Ag 3p (b), Cr 2p (c), and N 1s (d) core level XPS spectra of the recycled catalyst AgCr@CN-800-R4.

12. CHARACTERIZATION DATA AND EXPERIMENTAL DETAILS OF THE ISOLATED PRODUCTS

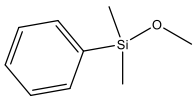

Dimethyl(phenyl)silane (3aa): Yield: 89 %. Product purify by silica gel column chromatography using *n*-hexane/ethyl acetate mixtures as the eluent solvent. The NMR spectrum is consistent with the reported data.[5] ^{1}H NMR (400 MHz, $CDCl_3$) δ 7.66 – 7.55 (m, 2H), 7.48 – 7.33 (m, 3H), 3.47 (s, 3H), 0.41 (s, 6H). ^{13}C NMR (101 MHz, $CDCl_3$) δ 137.80, 133.79, 129.97, 128.21, 50.97, -2.00. ^{29}Si NMR (79 MHz, $CDCl_3$) δ 9.41. MS (EI): *m*/*z* (rel. int.) 166.

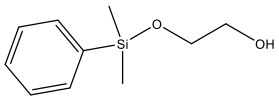

2-((dimethyl(phenyl)silyl)oxy)ethan-1-ol (3ai): Yield: 79 %. After removing the catalyst by filtration, the product was extracted with *n*-hexane and purify by silica gel column chromatography using *n*-hexane/ethyl acetate mixtures as the eluent solvent. ^{1}H NMR (400 MHz, $CDCl_3$) δ 7.64 – 7.53 (m, 2H), 7.46 – 7.34 (m, 3H), 3.74 – 3.61 (m, 5H), 0.42 (s, 6H). ^{13}C NMR (101 MHz, $CDCl_3$) δ 137.70, 133.73, 130.10, 128.28, 64.40, 63.92, -1.59. ^{29}Si NMR (79 MHz, $CDCl_3$) δ 9.28. MS (EI): *m*/*z* (rel. int.) 196.

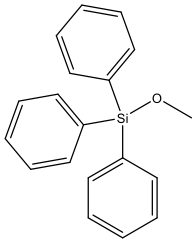

Metoxytriphenylsilane (3ba): Yield: 93 %. Product obtained by solvent evaporation. The NMR spectrum is consistent with the reported data.[6] ^{1}H NMR (300 MHz, $CDCl_3$) δ 7.92 (dd, *J* = 7.6, 1.9 Hz, 6H), 7.75 – 7.50 (m, 9H), 3.89 (s, 3H). ^{13}C NMR (75 MHz, $CDCl_3$) δ 135.66, 134.20, 130.35, 128.19, 52.07. ^{29}Si NMR (79 MHz, $CDCl_3$) δ -11.33. MS (EI): *m*/*z* (rel. int.) 290.

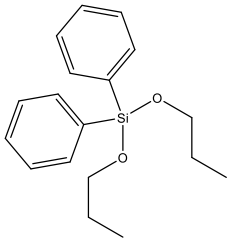

Diphenyldipropoxysilane (3cc): Yield: 92 %. Product purify by silica gel flash chromatography using *n*-hexane as the eluent solvent. The NMR spectrum is consistent with the reported data.[7] ^{1}H NMR (300 MHz, $CDCl_3$) δ 7.80 (dd, *J* = 7.7, 1.9 Hz, 4H), 7.62 – 7.33 (m, 6H), 3.88 (t, *J* = 6.6 Hz, 4H), 1.75 (d, *J* =

7.4 Hz, 4H), 1.05 (t, *J* = 7.4 Hz, 6H). ^{13}C NMR (75 MHz, $CDCl_3$) δ 135.03, 133.43, 130.23, 127.89, 64.93, 25.84, 10.43. ^{29}Si NMR (79 MHz, $CDCl_3$) δ -32.73. MS (EI): *m*/*z* (rel. int.) 300.

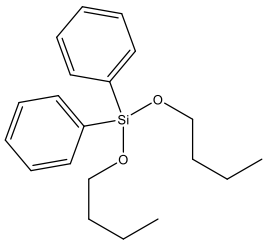

Dibutoxydiphenylsilane (3cd): Yield: 80 %. Product purify by silica gel flash chromatography using *n*-hexane as the eluent solvent. The NMR spectrum is consistent with the reported data.[8] ^{1}H NMR (300 MHz, $CDCl_3$) δ 7.71 (dd, J = 7.7, 1.8 Hz, 4H), 7.62 – 7.30 (m, 6H), 3.84 (t, J = 6.5 Hz, 4H), 1.76 – 1.54 (m, 4H), 1.54 – 1.34 (m, 4H), 0.94 (t, J = 7.3 Hz, 6H). ^{13}C NMR (75 MHz, $CDCl_3$) δ 135.05, 133.46, 130.23, 127.90, 63.02, 34.77, 19.12, 13.98. ^{29}Si NMR (79 MHz, $CDCl_3$) δ -32.71. MS (EI): *m*/*z* (rel. int.) 328.

13. REFERENCES

1. Cerón Calloso, M.; Angulo-Cornejo, J. R.; Lino-Pacaheco, M. N.; Villanueva Huerta, C. C.; Casimiro Soriano, E. M., Synthesis and characterization of silver(I) complex with mixed ligands saccharinate and 2-(2-pyridyl)bezimidazole. *Rev. Colomb. Quim.* **2018,** *47*, 73-78.
2. Zhang, L.; Wang, A.; Wang, W.; Huang, Y.; Liu, X.; Miao, S.; Liu, J.; Zhang, T., Co–N–C Catalyst for C–C Coupling Reactions: On the Catalytic Performance and Active Sites. *Acs Catal.* **2015,** *5* (11), 6563-6572.
3. Bulushev, D. A.; Chuvilin, A. L.; Sobolev, V. I.; Stolyarova, S. G.; Shubin, Y. V.; Asanov, I. P.; Ishchenko, A. V.; Magnani, G.; Riccò, M.; Okotrub, A. V.; Bulusheva, L. G., Copper on carbon materials: stabilization by nitrogen doping. *J. Mater. Chem. A* **2017,** *5* (21), 10574-10583.
4. Tang, C.; Surkus, A.-E.; Chen, F.; Pohl, M.-M.; Agostini, G.; Schneider, M.; Junge, H.; Beller, M., A Stable Nanocobalt Catalyst with Highly Dispersed CoNx Active Sites for the Selective Dehydrogenation of Formic Acid. *Angew. Chem. Int. Ed.* **2017,** *56* (52), 16616-16620.
5. Mitsudome, T.; Yamamoto, Y.; Noujima, A.; Mizugaki, T.; Jitsukawa, K.; Kaneda, K., Highly Efficient Etherification of Silanes by Using a Gold Nanoparticle Catalyst: Remarkable Effect of O_2. *Chem. Eur. J.* **2013,** *19* (43), 14398-14402.
6. Luo, N.; Liao, J.; Ouyang, L.; Wen, H.; Zhong, Y.; Liu, J.; Tang, W.; Luo, R., Highly Selective Hydroxylation and Alkoxylation of Silanes: One-Pot Silane Oxidation and Reduction of Aldehydes/Ketones. *Organometallics* **2020,** *39* (1), 165-171.

7. Reuter, M. B.; Cibuzar, M. P.; Hammerton, J.; Waterman, R., Photoactivated silicon–oxygen and silicon–nitrogen heterodehydrocoupling with a commercially available iron compound. *Dalton Trans.* **2020,** *49* (9), 2972-2978.
8. Blandez, J. F.; Primo, A.; Asiri, A. M.; Álvaro, M.; García, H., Copper Nanoparticles Supported on Doped Graphenes as Catalyst for the Dehydrogenative Coupling of Silanes and Alcohols. *Angew. Chem. Int. Ed.* **2014,** *53* (46), 12581-12586.

14. ^{1}H, ^{13}C, AND ^{29}Si NMR SPECTRA OF THE ISOLATED PRODUCTS

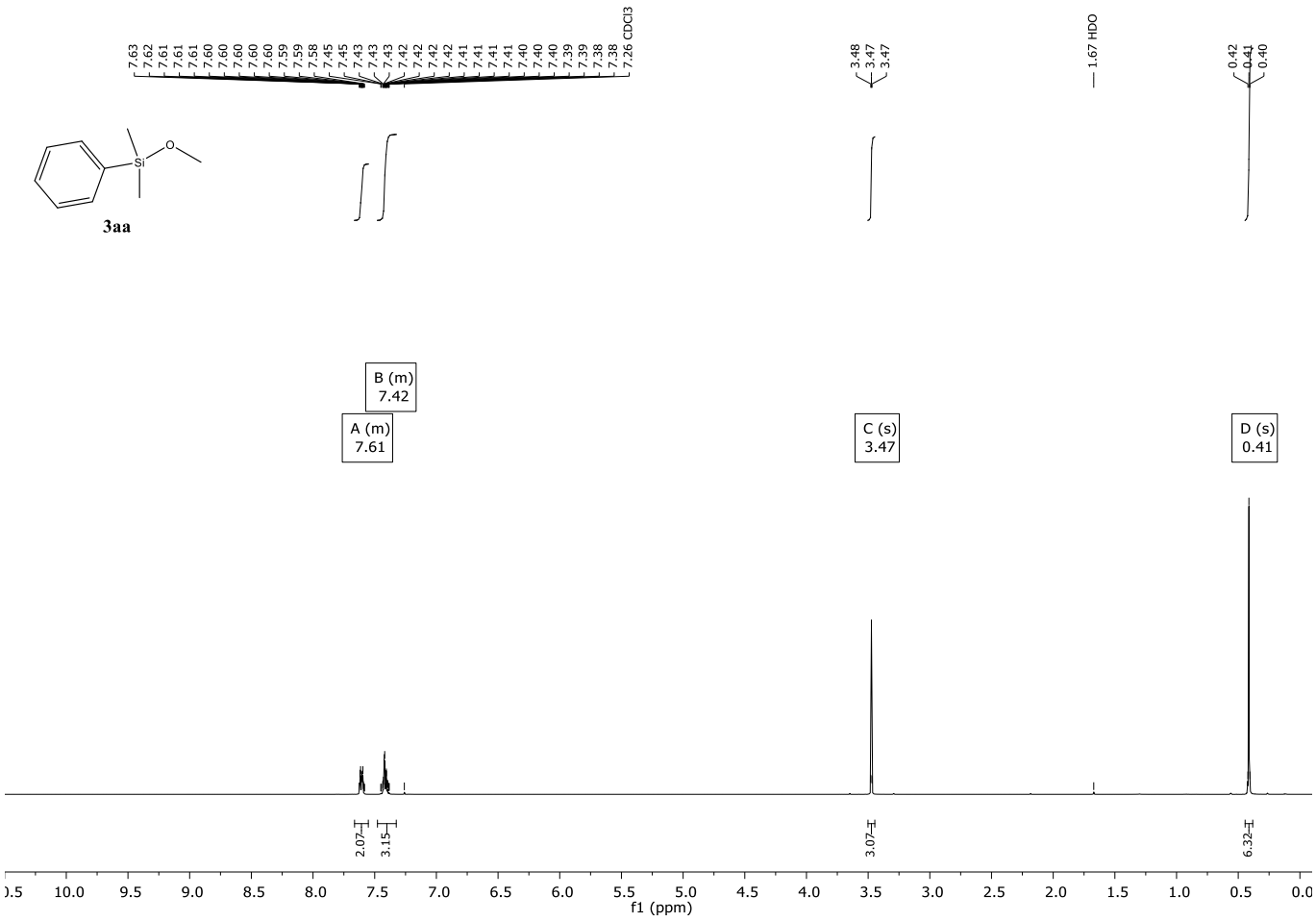
7.63 7.62 7.61 7.61 7.61 7.60 7.60 7.60 7.60 7.59 7.59 7.58 7.45 7.43 7.43 7.42 7.42 7.42 7.41 7.41 7.41 7.40 7.40 7.39 7.39 7.38 7.38 7.26 CDCl3
3.48 3.47 3.47
1.67 HDO
0.42 0.41 0.40
Si
O
3aa
B (m) 7.42
A (m) 7.61
C (s) 3.47
D (s) 0.41
2.07
3.15
3.07
6.32
f1 (ppm)

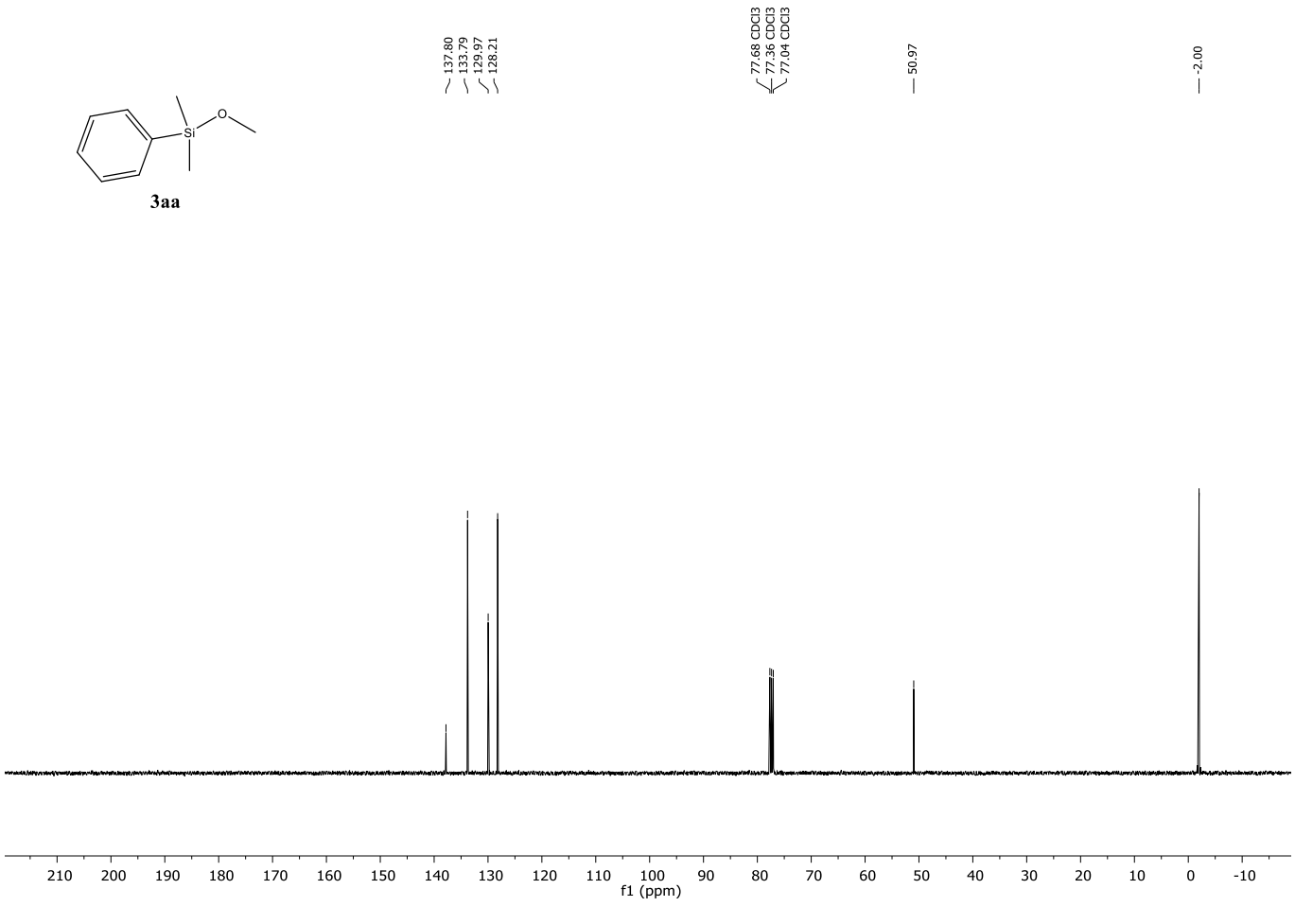
137.80 133.79 129.97 128.21
77.68 CDCl3 77.36 CDCl3 77.04 CDCl3
50.97
-2.00
Si
O
3aa
f1 (ppm)

— 9.41

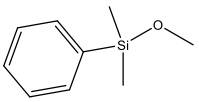
Si
O

3aa

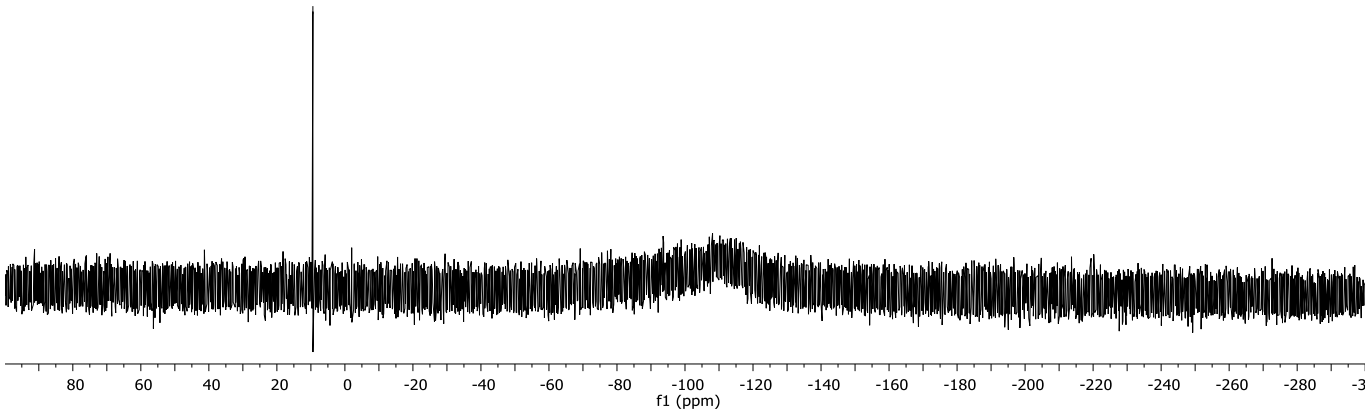
80
60
40
20
0
-20
-40
-60
-80
-100
-120
-140
-160
-180
-200
-220
-240
-260
-280
-3
f1 (ppm)

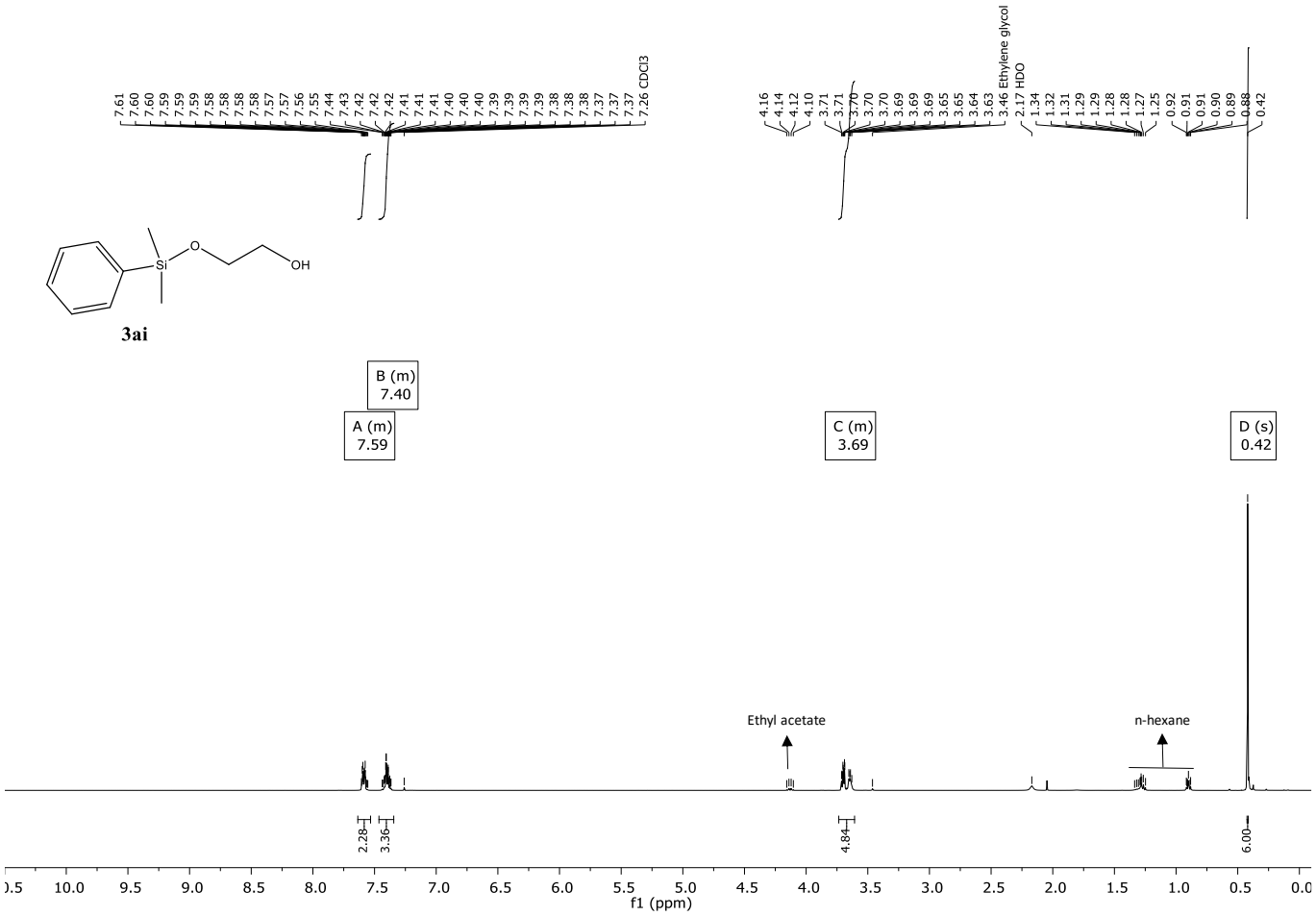
7.61 7.60 7.60 7.59 7.59 7.59 7.58 7.58 7.58 7.58 7.57 7.57 7.56 7.55 7.44 7.43 7.42 7.42 7.42 7.41 7.41 7.41 7.40 7.40 7.40 7.39 7.39 7.39 7.39 7.38 7.38 7.38 7.37 7.37 7.37 7.26 CDCl3
4.16 4.14 4.12 4.10 3.71 3.71 3.70 3.70 3.70 3.69 3.69 3.69 3.65 3.65 3.64 3.63 3.46 Ethylene glycol 2.17 HDO 1.34 1.32 1.31 1.29 1.29 1.28 1.28 1.27 1.25 0.92 0.91 0.91 0.90 0.89 0.88 0.42
Si
O
OH
3ai
B (m) 7.40
A (m) 7.59
C (m) 3.69
D (s) 0.42
Ethyl acetate
n-hexane
2.28
3.36
4.84
6.00
f1 (ppm)

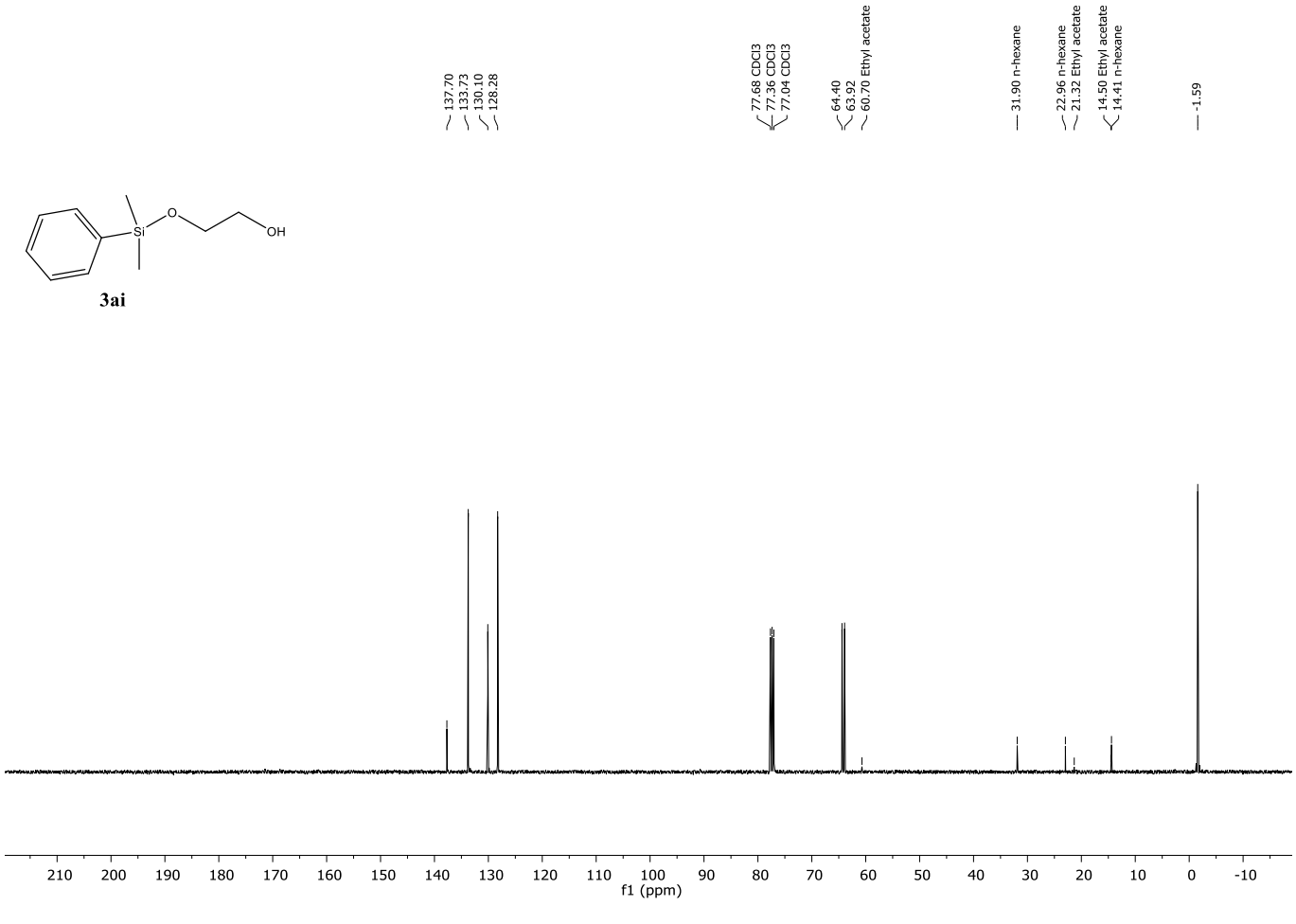
137.70 133.73 130.10 128.28
77.68 CDCl3 77.36 CDCl3 77.04 CDCl3
64.40 63.92 60.70 Ethyl acetate
31.90 n-hexane
22.96 n-hexane 21.32 Ethyl acetate
14.50 Ethyl acetate 14.41 n-hexane
-1.59
Si
O
OH
3ai
f1 (ppm)

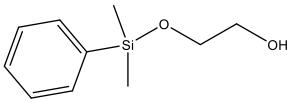
Si
O
OH

3ai

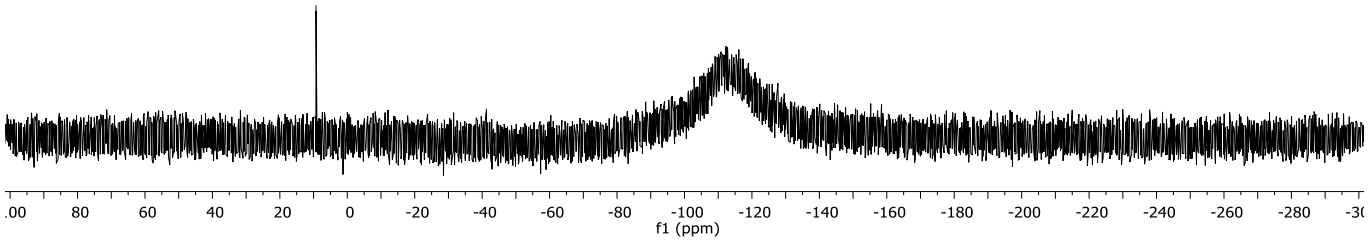
9.28
80
60
40
20
0
-20
-40
-60
-80
-100
-120
-140
-160
-180
-200
-220
-240
-260
-280
f1 (ppm)

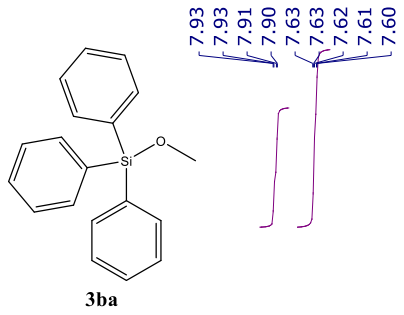
7.93
7.93
7.91
7.90
7.63
7.63
7.62
7.61
7.60
3.89
Si
O

3ba

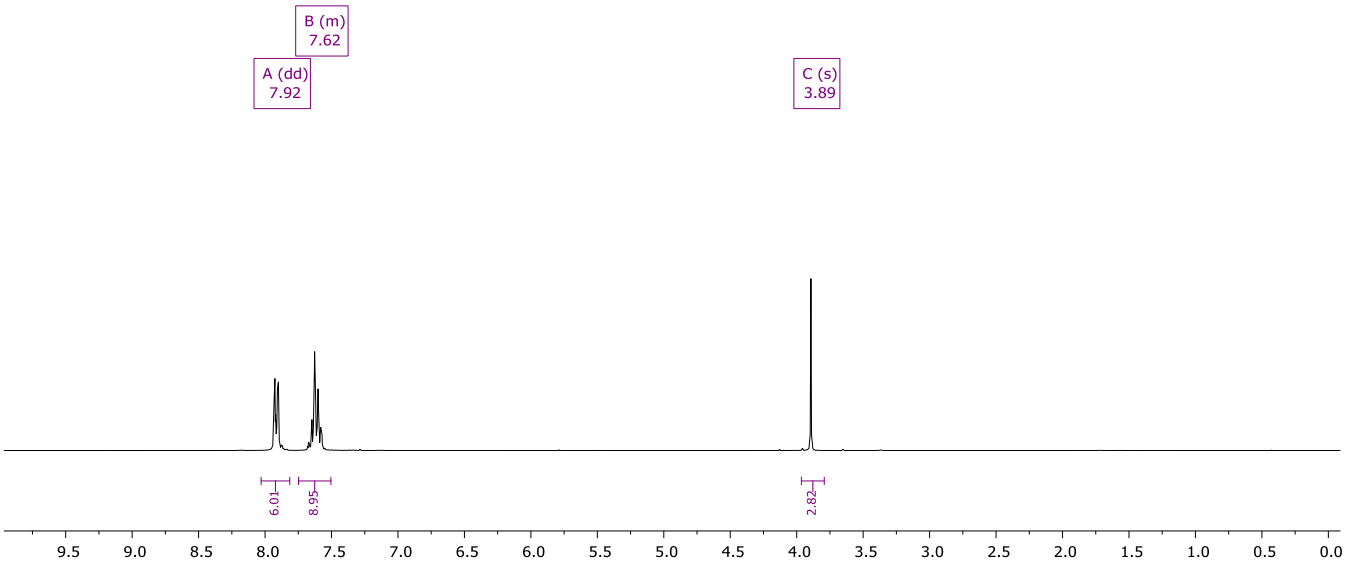
B (m)
7.62
A (dd)
7.92
C (s)
3.89
6.01
8.95
2.82
9.5
9.0
8.5
8.0
7.5
7.0
6.5
6.0
5.5
5.0
4.5
4.0
3.5
3.0
2.5
2.0
1.5
1.0
0.5
0.0

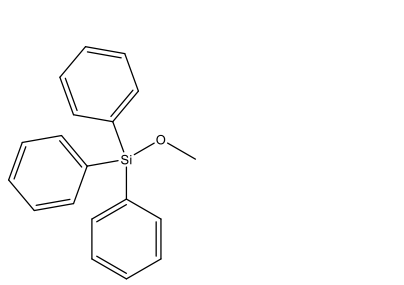
135.66
134.20
130.35
128.19
52.07
Si
O

3ba

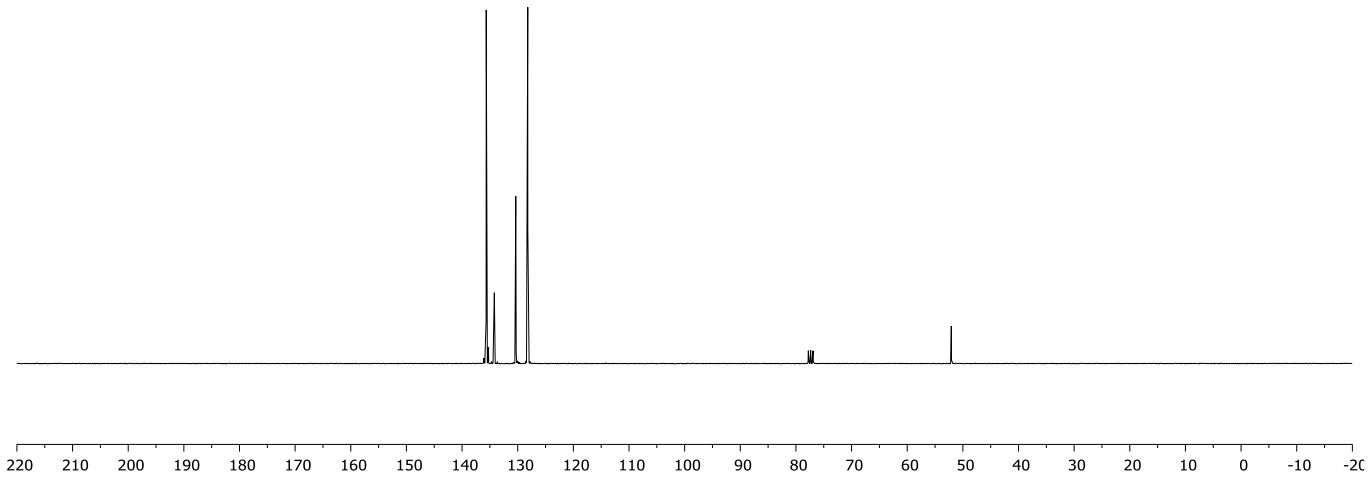
220
210
200
190
180
170
160
150
140
130
120
110
100
90
80
70
60
50
40
30
20
10
0
-10

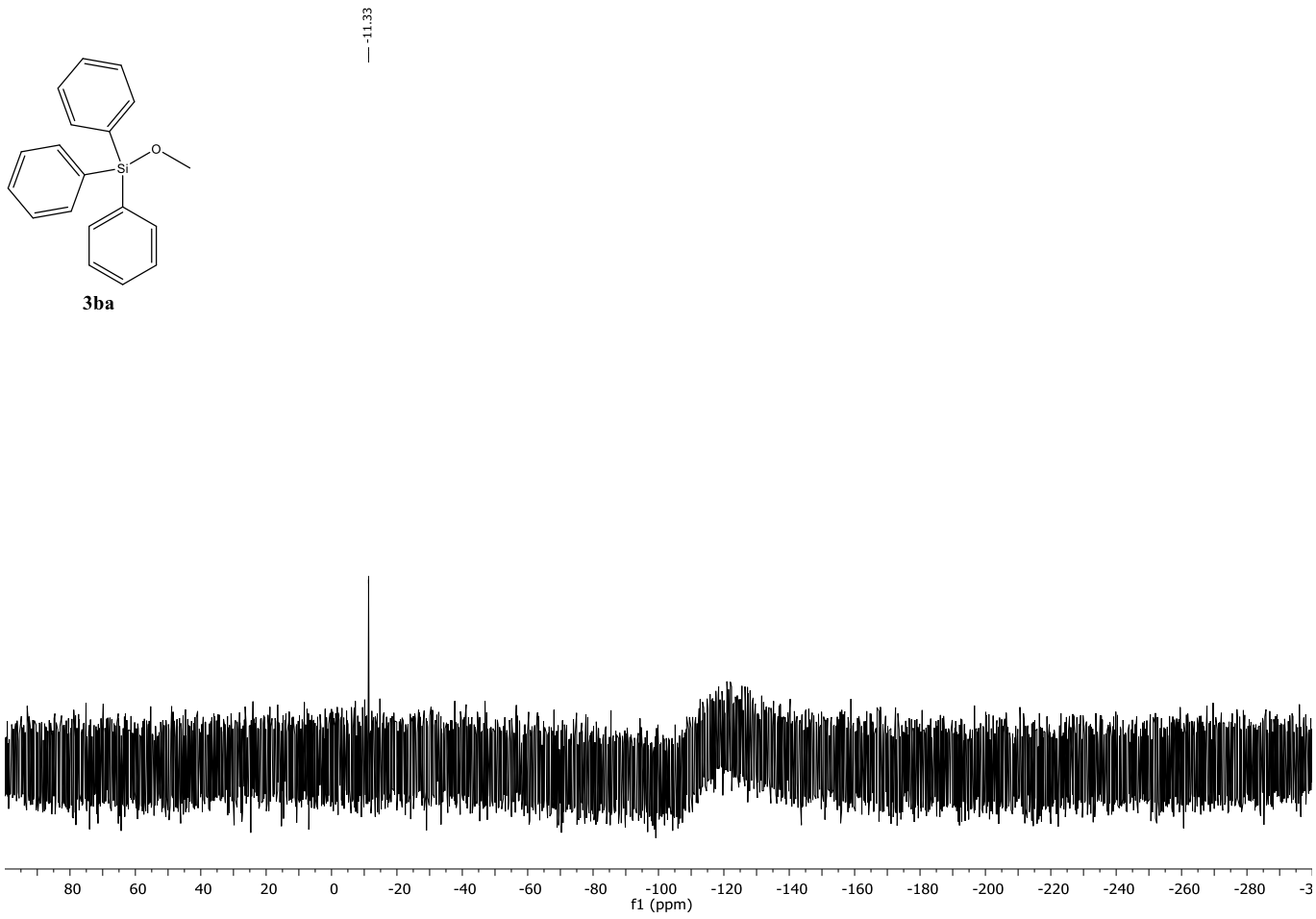
-11.33
Si
O
80
60
40
20
0
-20
-40
-60
-80
-100
-120
-140
-160
-180
-200
-220
-240
-260
-280
f1 (ppm)

3ba

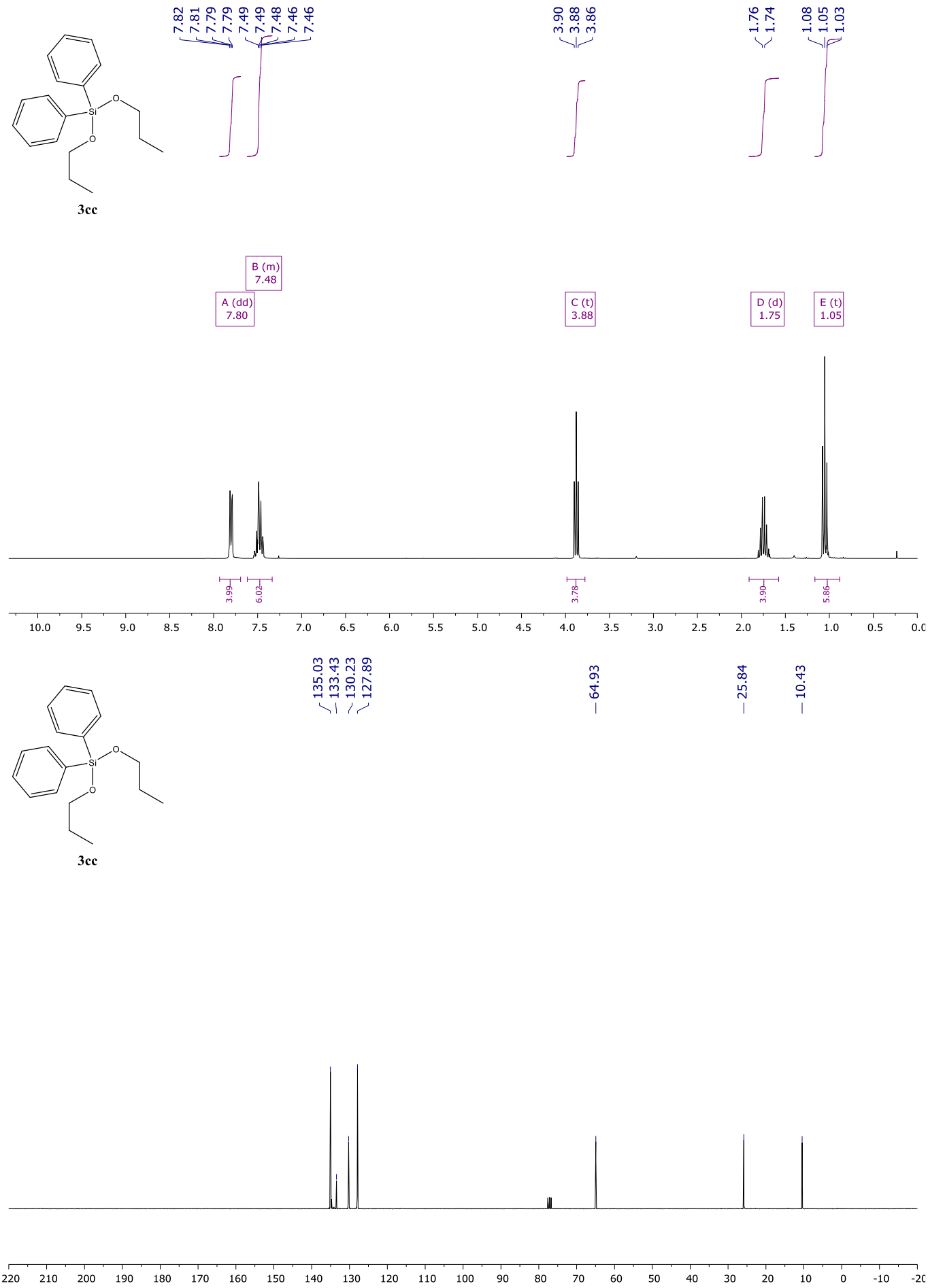
7.82
7.81
7.79
7.79
7.49
7.49
7.48
7.46
7.46
3.90
3.88
3.86
1.76
1.74
1.08
1.05
1.03
Si
O
O
3cc
B (m)
7.48
A (dd)
7.80
C (t)
3.88
D (d)
1.75
E (t)
1.05
3.99
6.02
3.78
3.90
5.86
10.0
9.5
9.0
8.5
8.0
7.5
7.0
6.5
6.0
5.5
5.0
4.5
4.0
3.5
3.0
2.5
2.0
1.5
1.0
0.5
135.03
133.43
130.23
127.89
64.93
25.84
10.43
Si
O
O
3cc
220
210
200
190
180
170
160
150
140
130
120
110
100
90
80
70
60
50
40
30
20
10
0
-10

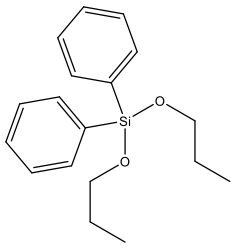
Si
O
O

3cc

-32.73
80
60
40
20
0
-20
-40
-60
-80
-100
-120
-140
-160
-180
-200
-220
-240
-260
-280
f1 (ppm)

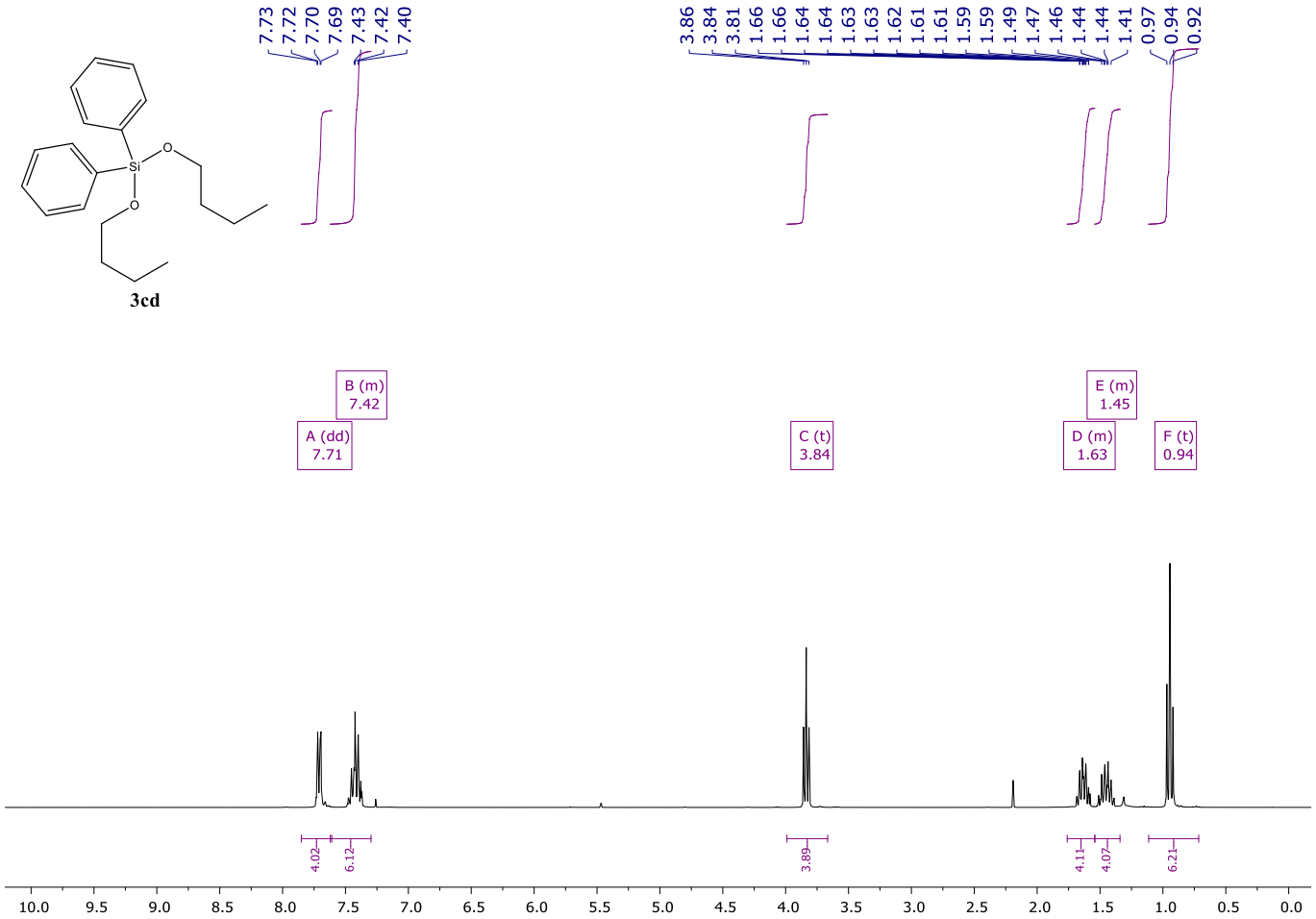
7.73
7.72
7.70
7.69
7.43
7.42
7.40
3.86
3.84
3.81
1.66
1.66
1.64
1.64
1.63
1.63
1.62
1.61
1.61
1.59
1.59
1.49
1.47
1.46
1.44
1.44
1.41
0.97
0.94
0.92
Si
O
O
3cd
B (m)
7.42
A (dd)
7.71
C (t)
3.84
E (m)
1.45
D (m)
1.63
F (t)
0.94
4.02
6.12
3.89
4.11
4.07
6.21
10.0
9.5
9.0
8.5
8.0
7.5
7.0
6.5
6.0
5.5
5.0
4.5
4.0
3.5
3.0
2.5
2.0
1.5
1.0
0.5
0.0

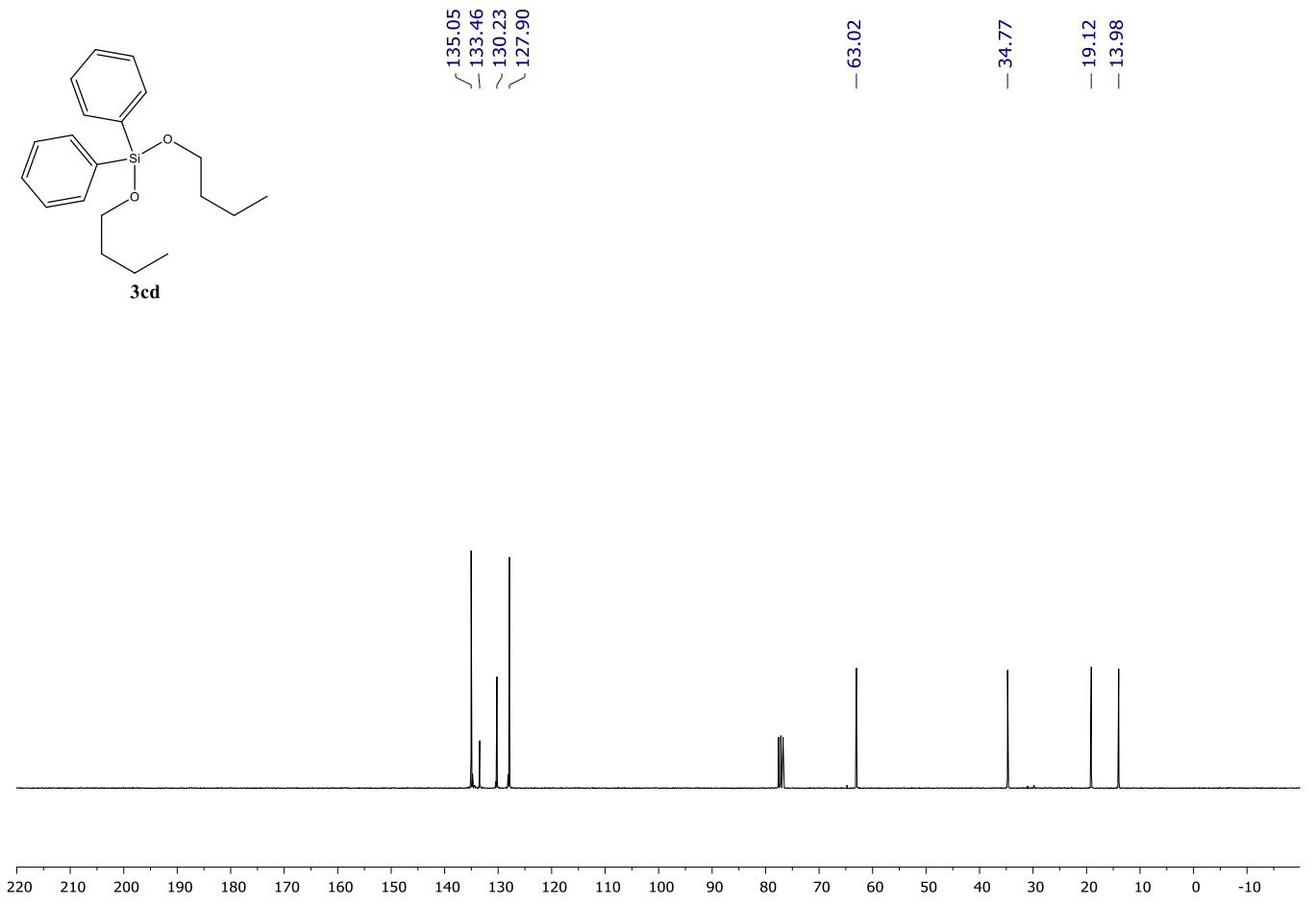
135.05
133.46
130.23
127.90
63.02
34.77
19.12
13.98
Si
O
O
3cd
220
210
200
190
180
170
160
150
140
130
120
110
100
90
80
70
60
50
40
30
20
10
0
-10

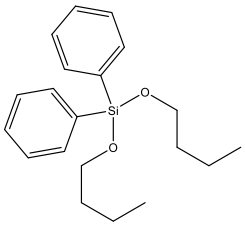
Si
O
O

3cd

-32.71
80
60
40
20
0
-20
-40
-60
-80
-100
-120
-140
-160
-180
-200
-220
-240
-260
-280
-3
f1 (ppm)